

## Preparation of nano-cellulose/ $\alpha$ -Fe<sub>2</sub>O<sub>3</sub> hybrid nanofiber for the cationic dyes removal: optimization characterization, kinetic, isotherm and error analysis

Gh. Chizari Fard<sup>1</sup>, M. Mirjalili<sup>1\*</sup>, F. Najafi<sup>2</sup>

<sup>1</sup>Department of Textile, Yazd Branch, Islamic Azad University, Yazd, Iran

<sup>2</sup>Department of Resin and Additives, Institute for Color Science and Technology, Tehran, Iran

Submitted March 24, 2016; Accepted August 8, 2016

In this paper, cellulose nanoparticle with the average diameter of 35.2 nm was synthesized through the hydrolysis of microcrystalline cellulose and incorporated onto the  $\alpha$ -Fe<sub>2</sub>O<sub>3</sub> nanofiber surface by citric acid to prepare a hybrid nanofiber. Then, the ability of the resultant nanofibers for the removal of cationic dyes was investigated. Also, the cross linking procedure with citric acid was optimized. The characterization analyses of synthesized nanofibers showed that the cellulose nanoparticles were successfully crosslinked together through the formation of ester linkages and they were deposited onto the surface of  $\alpha$ -Fe<sub>2</sub>O<sub>3</sub> nanofibers. A uniform distribution of cellulose nanoparticles along with some aggregations on the surface of nanofibers was observed which was depended on the citric acid content. Also, increasing the amount of citric acid resulted to increase the specific surface area values because of attaching the higher amounts of nanoparticles with high specific surface area value (480.65m<sup>2</sup>/g) onto the nanofiber surface. Furthermore, the effects of nanofiber dosage, initial dye concentration, and solution pH on the dye removal were studied. It was found that adsorption of dye process is highly pH-dependent. In order to evaluate the rate and mechanism of adsorption, the kinetic and isotherm models were studied. To do these, non-linear regression along with 3 error functions was used to determine the best fit model. It was concluded that adsorption of dyes follows with Langmuir isotherm. In addition, adsorption kinetic conforms to pseudo-second order model.

**Key words:**  $\alpha$ -Fe<sub>2</sub>O<sub>3</sub>, dye removal, cellulose nanoparticle, surface modification, adsorption kinetic, isotherm

### INTRODUCTION

Colored wastewater, as a consequence of dye usage in the textile and other industries, is highly toxic, carcinogenic, mutagenic, and may effect on aquatic life even at low concentrations significantly. Thus, the removal of dyes from waste effluents has become important. Several processes such as, nano-filtration [1], ozonation [2], coagulation [3], electrocoagulation [4], photocatalytic degradation [5] and adsorption [6, 7] were used to remove dyes from liquid phase. Among them, adsorption method is found to be more effective for the removal of dyes. Also, it is known as a simple, easy to operate and low-cost method. Different adsorbents have been used for removing of dyes from aqueous solutions such as magnetite [8] silica gels [9], fly ash [10], peat [11], activated carbon [12], clays [13], chitosan [14], alginate [15], etc. Many of these adsorbents are easily available but they have some disadvantages such as poor mechanical resistance, high cost of production and regeneration and relatively limited adsorption capacity for dyes.

The iron-based materials are of great interest for researchers which were used in many fields, such as magnetic fluids, data storage, catalysis, bio applications and water treatment [16]. Ferrihydrite, akaganeite, goethite, hematite, lepidocrocite and

magnetite are the iron oxides and hydroxides that have been used in water treatment systems [17]. Among them, hematite is the most stable and abundant iron oxide, found in soil and sediments and is widely used in water purification compared to the other iron based materials [18].

In the adsorption process, the main factor affecting on adsorption efficiency is the interaction between adsorbate and the functional groups present on the adsorbent surface. The combination of organic and inorganic components can increase the number of surface functional groups and consequently enhance the dye adsorption property. In this regard, surfactant, polymer and monomer are used for this purpose [19]. Amine-functionalized silica, amine-functionalized magnetic ferrite, aldehyde functionalized Fe<sub>2</sub>O<sub>3</sub>, iron oxide magnetic functionalized by lipophilic stilbene molecules, iron-chitosan composite, amino-functionalized Fe<sub>3</sub>O<sub>4</sub>-SiO<sub>2</sub>, Surfactant-modified bentonite and polyacrylic acid modified magnetic mesoporous carbon are synthesized and used for water treatment [20-27].

Cellulose is one of the most abundant natural biopolymers that is known as a non-toxic, low cost, and biodegradable material. Due to the presence of hydroxyl groups, cellulose is a promised material for surface modification [28]. Cross-linked cellulose-epichlorohydrin polymer, amine functionalized cellulose nanocrystal and polyethylenimine grafted

\* To whom all correspondence should be sent:  
E-mail: Dr.mirjalili@iauyazd.ac.ir

cellulose copolymer are prepared and their adsorption behaviour are investigated [29- 31] . Previously,  $\alpha$ -Fe<sub>2</sub>O<sub>3</sub> nanofiber is synthesized and used as an adsorbent for the removal of dyes and heavy metal ions [32, 33] . However, the adsorption capacity of synthesized nanofibers was low owing to the limited adsorption sites. This limits its application in the practical treatment of pollutants [34]. In order to improve the adsorption capacity, it is necessary to modify  $\alpha$ -Fe<sub>2</sub>O<sub>3</sub> nanofibers. A combination of bioadsorbents and iron oxide could possibly prepare an adsorbent with high adsorption capacity. A literature review showed that the nano cellulose/ $\alpha$ -Fe<sub>2</sub>O<sub>3</sub> nanofiber (hereafter; Cell/Fe<sub>2</sub>O<sub>3</sub> NF) was not synthesized and its dye removal ability was not investigated. In this study,  $\alpha$ -Fe<sub>2</sub>O<sub>3</sub> nanofiber was prepared by electrospinning technique and cellulose nanoparticle (hereafter; Cell NP) was incorporated onto the surface of nanofiber by citric acid (CA) to prepare a hybrid nanofiber. In order to optimize the adsorption condition, the effects of initial pH, initial dye concentration and nanofiber dosage on dye removal was investigated. Also, the adsorption kinetic and isotherm were studied.

## EXPERIMENTAL SECTION

### Materials

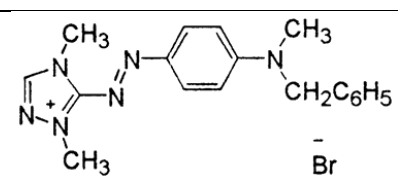
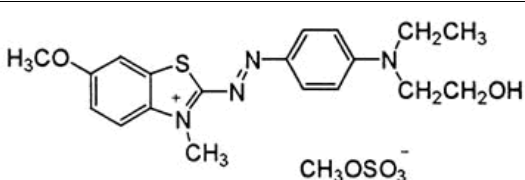
Poly vinyl alcohol (PVA) (degree of polymerization: 600, saponification value: 88.1 mol%), ferric nitrate (Fe(NO<sub>3</sub>)<sub>3</sub>.9H<sub>2</sub>O, 98%), 2

propanol, citric acid (CA), sodium hypophosphite (SHP), Sulfuric acid (98% w/w), hydrochloric acid (37% w/w) and tetraethyl orthosilicate (TEOS) were all purchased from Merck, Germany. Commercial microcrystalline cellulose (average particle size: 20  $\mu$ m) was purchased from Sigma-Aldrich. Two commercial cationic dyes, C.I. Basic red 46 (BR46) and C.I. Basic blue 41 (BB41) were obtained from Alvan Sabet Co. Iran and used without further purification. The characteristic and chemical structures of dyes are given in Table 1.

### Preparation of $\alpha$ -Fe<sub>2</sub>O<sub>3</sub> nanofiber

PVA solution (10% w/w) was prepared by dissolving PVA (1g) in distilled water (10mL) at 90°C with constant stirring for 4h. Then, 0.4g of ferric nitrate was added to the PVA solution and the stirring was continued for 6h. The prepared electrospinning solution was loaded into a plastic syringe with an 18-gauge stainless steel needle. The electrospinning apparatus was a Gamma High Voltage Research RR60 power supply and nanofibers were collected onto aluminum (Al) sheet. The distance between the needle tip and collector, electrical field and the feeding rate of the polymer solution were 15cm, 18kV and 0.3 mL/h, respectively. All electrospinning processes were carried out at room temperature. The electrospun nanofibers were dried at 60°C for 6h and calcined at 500°C for 3h in air to get  $\alpha$ -Fe<sub>2</sub>O<sub>3</sub> nanofibers at a heating rate of 5°C/min.

**Table 1.** Characteristic and chemical structures of dyes

| Name          | Formula  | M <sub>w</sub><br>(g/mol) | $\lambda_{max}$ (nm) | Chemical structures  |
|---------------|--|---------------------------|----------------------|--|
| Basic red 46  | C <sub>18</sub> H <sub>21</sub> BrN <sub>6</sub>                             | 401.3                     | 530                  |  |
| Basic blue 41 | C <sub>20</sub> H <sub>26</sub> N <sub>4</sub> O <sub>6</sub> S <sub>2</sub> | 482.57                    | 617                  |  |

### Preparation of Cell NP

Preparation of Cell NP was conducted according to Wang et al. [35]. Briefly, microcrystalline cellulose was hydrolyzed in a mixture of Sulfuric acid, hydrochloric acid, and distilled water at a ratio of 3:1:6 (v/v) under ultrasonic treatment for 10h. After hydrolysis, the acid was thoroughly removed

by washing, centrifugation, and dialysis with distilled water until the pH of washing water reached 5.

### Preparation of Cell/ $\alpha$ -Fe<sub>2</sub>O<sub>3</sub> hybrid nanofibers

In order to perform a successful incorporation of cell NP onto the nanofiber surface, it was necessary to increase the number of hydroxyl group on the

nanofiber surface. To do this, a silica gel with the molar composition of TEOS:HCl:H<sub>2</sub>O=1:2:0.07 was produced by hydrolysis and polycondensation from the dropwise addition of aqueous HCl to TEOS with vigorous stirring for 1h. Then, the  $\alpha$ -Fe<sub>2</sub>O<sub>3</sub> nanofibers were soaked into the prepared solution for 2h. After that, the nanofiber dried at 60°C and washed with deionized water: ethanol with the ratio of 2:1. The process of incorporation of Cell NP on the nanofiber surface was conducted as follows: 0.5g of synthesized nanofiber was added in a mixture containing 0.5g cellulose nanoparticle, 20mL deionized water and different amounts of CA (0.01-0.08g) and SHP (the mass ratio of CA:SHP was 2:1) and the mixture was subjected to ultrasonic treatment for 10min. Then, the mixture was stirred at 75°C. After the complete evaporation of solvent, the nanofibers were placed in an oven at 140°C for 15min. Finally, nanofibers were washed 5 times by successive agitations/centrifugations with deionized water to remove unattached and self-crosslinked cellulose nanoparticles.

#### Characterization

The FTIR spectra of  $\alpha$ -Fe<sub>2</sub>O<sub>3</sub> and Cell/Fe<sub>2</sub>O<sub>3</sub> NF were examined by the FTIR spectroscopy (ThermoNicolet NEXUS 870 FTIR from Nicolet Instrument Corp., USA). The surface morphology of nanofibers was investigated using a Scanning Electron Microscope (SEM, LEO1455VP, and ENGLAND). Surface area measurement of the nanofibers was carried out using a Brunauer–Emmett–Teller (BET) analyzer (Micromeritics Gemini III 2375, USA). The point of zero charge (pH<sub>PZC</sub>) of the prepared adsorbent was determined by the solid addition method [36]. The average diameter of Cell NP and  $\alpha$ -Fe<sub>2</sub>O<sub>3</sub> NF were determined by an image processor (SXM-196X).

#### Adsorption studies

Batch adsorption experiments were carried out by mixing the Cell/Fe<sub>2</sub>O<sub>3</sub> NF with 200 mL of dye solutions (30 mg·L<sup>-1</sup>) at pH of 9 for 60 min. The residual dye concentration was determined after different time intervals (5-60 min) by UV–VIS spectrophotometry (CECIL 2021). To do this, the absorbance of supernatant solution was monitored at 530 and 617 nm for BR46 and BB41, respectively. The pH of dye solution was adjusted to a desired value by dropwise adding 0.1 mol/L NaOH or 0.1 mol/L HCl solutions.

The effect of initial dye concentration on the dye removal was studied by adding 0.008 g of Cell/Fe<sub>2</sub>O<sub>3</sub> NF to different dye concentrations of 20, 30, 40, 50, and 60 mg·L<sup>-1</sup> of dye solutions (200 mL) at pH=9. The effect of adsorbent dosage on dye removal was

investigated by mixing different amounts of adsorbent (0.004-0.01gr) with 200 mL of BR46 and BB41, dye solutions (30mg·L<sup>-1</sup>) at pH of 9. The effect of pH on dye removal was evaluated by adding 0.008g adsorbent to 200 mL of dye solutions (30 mg·L<sup>-1</sup>) at different pH values (2, 3, 5, 7, 9 and 10).

The experiments were done three times. The standard deviation is <5%. The amount of dye adsorbed per unit mass of nanofiber (q) and the dye removal efficiency (R) were calculated according to Eqs. (1) and (2), respectively:

$$q = \frac{(C_0 - C_e) \times V}{M} \quad (1)$$

$$R\% = \frac{C_0 - C}{C_0} \times 100 \quad (2)$$

where C<sub>0</sub> and C<sub>e</sub> are the initial and the equilibrium concentrations of the dye in the solution (mg L<sup>-1</sup>), V is the volume of the solution (L), C is dye concentration at t = t and M is the weight of the adsorbent.

## RESULTS AND DISCUSSION

#### FTIR analysis

The FT-IR spectra of  $\alpha$ -Fe<sub>2</sub>O<sub>3</sub> and Cell/Fe<sub>2</sub>O<sub>3</sub> NF are shown in Fig. 1. In the spectrum of  $\alpha$ -Fe<sub>2</sub>O<sub>3</sub> nanofiber (curve A), the H-O-H stretching modes and bending vibration of the free or adsorbed water detected at 3419 and 1622 cm<sup>-1</sup>, respectively. Also, the characteristic peak of the stretching mode of Fe–O was seen at 531 cm<sup>-1</sup> [15], confirming the formation of  $\alpha$ -Fe<sub>2</sub>O<sub>3</sub> (hematite) [37]. In the spectrum of Cell NP incorporated nanofiber, the band observed at 1166 cm<sup>-1</sup> attributed to the anti-symmetric stretching vibrations of C–O–C bridge. The characteristic peak of glucosidic ring in cellulose was detected at 897 cm<sup>-1</sup>. Also, the band at 1430 cm<sup>-1</sup> is associated with the HCH and OCH in-plane bending vibration which is ascribed as a crystalline absorption band [38, 39]. The stretching and out of plane bending vibrations of OH groups detected at 3340 and 711 cm<sup>-1</sup>, respectively. The band at 1080 and 471cm<sup>-1</sup> are associated with the asymmetric and symmetric stretching vibrations of Si-O-Si bond, respectively [40]. Also, the band appeared at 533 cm<sup>-1</sup> attributed to the stretching vibration of Fe-O. As can be seen from Fig. 1B, the intensity of the band at 3340 cm<sup>-1</sup> increased after the incorporation of Cell NP on the surface, indicating the incorporation of high amounts of hydroxyl groups on the surface. Furthermore, a new band at 1725 cm<sup>-1</sup> was observed which is attributed to the stretching vibration of carbonyl of ester [41]. It was concluded that the Cell NP was crosslinked together by citric acid and the crosslinked nanoparticles were deposited onto the surface of  $\alpha$ -Fe<sub>2</sub>O<sub>3</sub> nanofiber due

to hydrogen bonds created between the OH groups of the deposited silica on the surface of nanofibers

and reactive groups of Cell NPs. The proposed reaction between components is illustrated at Fig. 2.

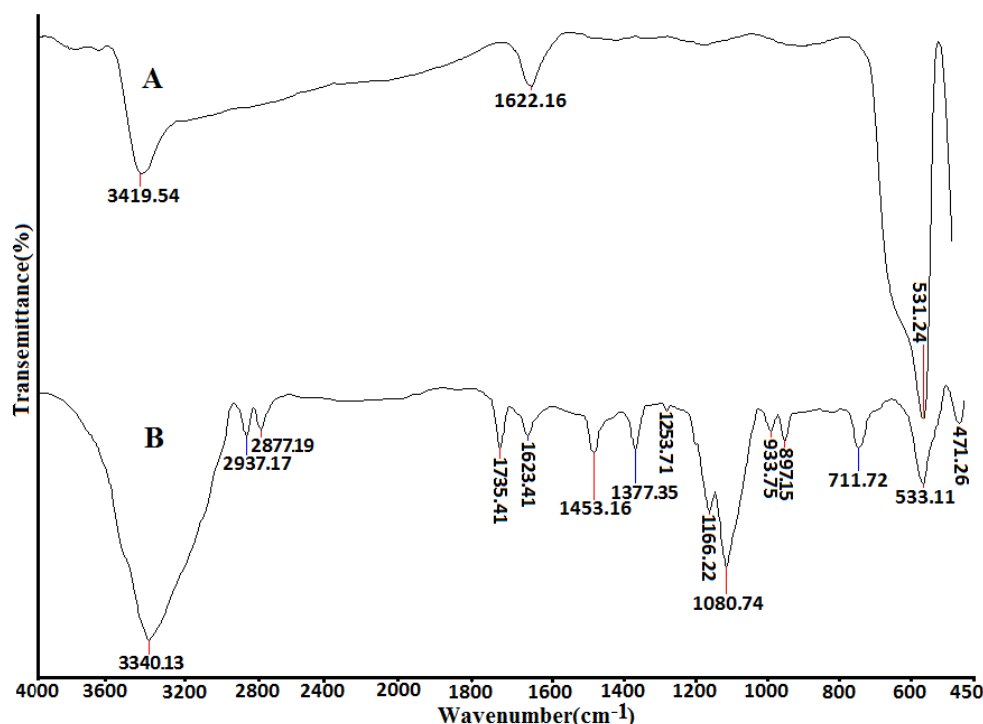


Fig. 1. The FTIR spectra of (A)  $\alpha$ -Fe<sub>2</sub>O<sub>3</sub> and (B) Cell/Fe<sub>2</sub>O<sub>3</sub> NF.

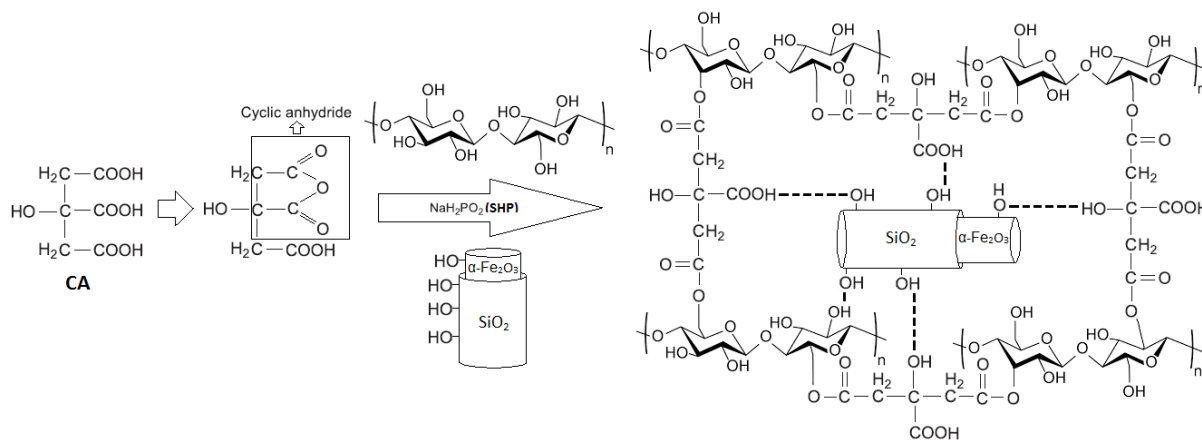


Fig. 2. The proposed reaction between components

#### Microscopic characterization

The SEM images of Cell NP,  $\alpha$ -Fe<sub>2</sub>O<sub>3</sub> and Cell/Fe<sub>2</sub>O<sub>3</sub> NF at different magnifications are shown in Fig. 3. The Cell NPs with a smooth surface appear irregular but overall spherical in shape (Fig. 3A). The  $\alpha$ -Fe<sub>2</sub>O<sub>3</sub> NF exhibited a rigid and long continuous structure (Fig. 3B). Size distribution diagrams of the Cell NP and  $\alpha$ -Fe<sub>2</sub>O<sub>3</sub> NFs are shown in Fig. 4. As can be seen, the dimensions of the Cell NPs and  $\alpha$ -Fe<sub>2</sub>O<sub>3</sub> NFs were distributed in the range of 10-100 and 60-140nm, respectively. Also, their average diameter were 35.2 and 92.6nm, respectively.

For Cell/Fe<sub>2</sub>O<sub>3</sub> NF, a relatively uniform distribution of Cell NP on the surface of nanofibers

was seen (Fig. 3E). Furthermore, the rigidity of nanofibers decreased after the incorporation process which is probably due to the amorphous nature of coated silica. According to the Fig. 3E, the presence of Cell NPs is more evident at touching point of nanofibers.

In order to achieve the highest adsorption efficiency, optimization of the incorporation process was carried out by varying the amount of citric acid in the range of 0.01-0.08g. The mass ratio of CA: SHP was kept at 2:1. As can be seen from the SEM images (Fig. 3C-F), with increasing the amount of CA in incorporation process the number of Cell NP attached to the surface of  $\alpha$ -Fe<sub>2</sub>O<sub>3</sub> NF increased. However, the structure of nanofibers was changed



when the amount of CA increased to 0.08g. As can be seen in Fig. 3F, the nanofibers were conglomerated together and also the Cell NP aggregated and formed large masses due to crosslinking role of citric acid. It was stated that polycarboxylic acids esterify the hydroxyl groups of the cellulosic chains through the

formation of cyclic anhydride intermediates [42]. For the hybrid nanofibers synthesized with 0.08g citric acid, all the voids existing among the nanofibers was filled by large masses of nanoparticles.

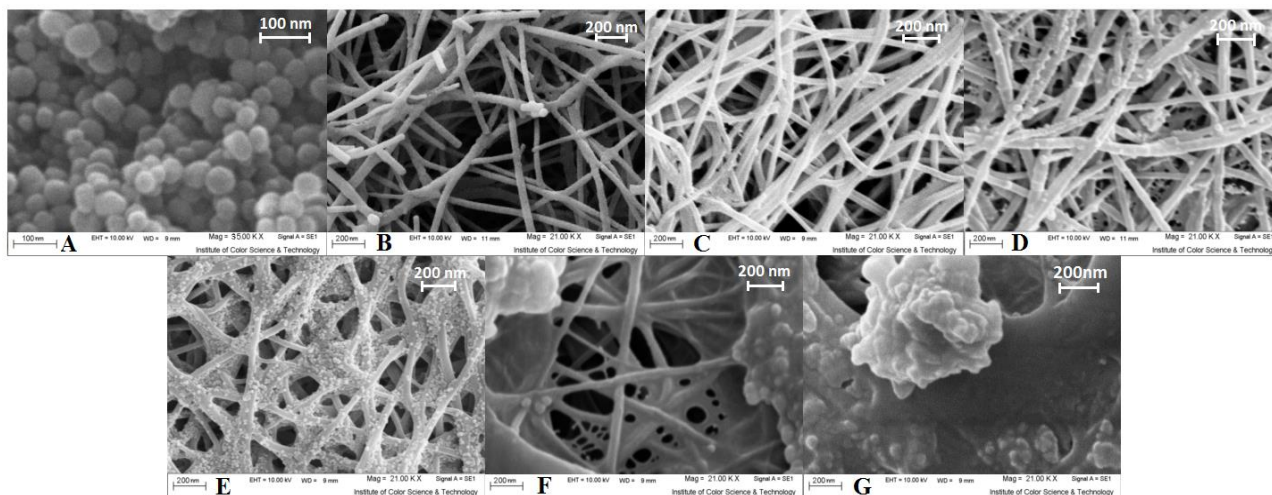


**Fig. 3.** The SEM images of (A) Cell NP, (B)  $\alpha$ -Fe<sub>2</sub>O<sub>3</sub> NF and (C) Cell/Fe<sub>2</sub>O<sub>3</sub> NFs (CA= 0.01 g), (D) Cell/Fe<sub>2</sub>O<sub>3</sub> NFs (CA= 0.03 g), (E) Cell/Fe<sub>2</sub>O<sub>3</sub> NFs (CA= 0.06 g), (F) Cell/Fe<sub>2</sub>O<sub>3</sub> NFs (CA= 0.07 g), (G) Cell/Fe<sub>2</sub>O<sub>3</sub> NFs (CA= 0.08 g),

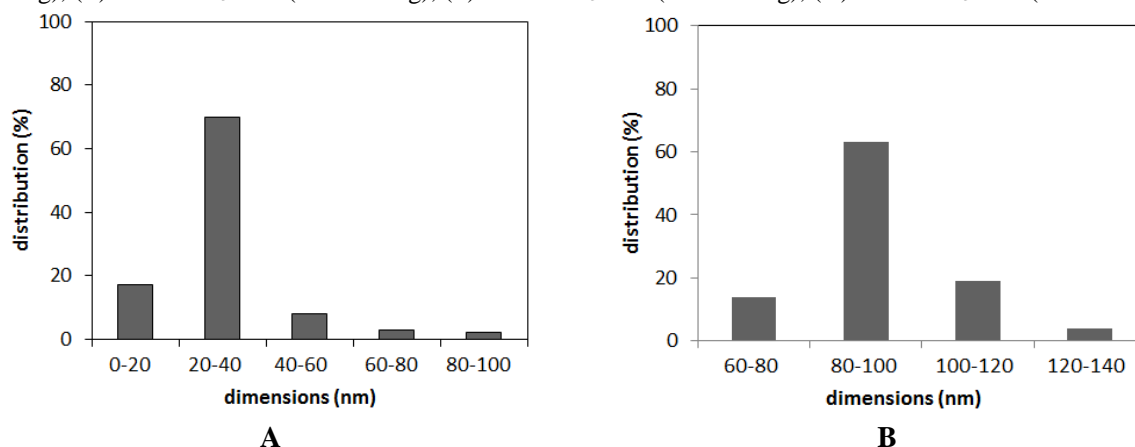


**Fig. 4.** Size distribution diagrams of the (A) Cell NP and (B)  $\alpha$ -Fe<sub>2</sub>O<sub>3</sub> NF

The BET surface area value of Cell/Fe<sub>2</sub>O<sub>3</sub> NF synthesized with different amounts of CA is shown in Table 2. The BET surface area value of Cell NP was 480.65m<sup>2</sup>/g. The aggregation of nanoparticles on the nanofiber surface caused to decrease the BET surface area values. From the Table 2, it was clear that the values were initially increased from 137.28 m<sup>2</sup>/g for  $\alpha$ -Fe<sub>2</sub>O<sub>3</sub> NF to 140.55 and 178.74m<sup>2</sup>/g for the samples synthesized with 0.01 and 0.06 g CA, respectively due to incorporation of Cell NP with high BET surface area value on the surface. After that, it was decreased to 41.73m<sup>2</sup>/g when the amount of CA increased to 0.08g by the reason of conglutination of nanofibers together, aggregation of nanoparticles on the surface and filling of voids among the nanofibers. In this regard, 0.06g CA was

selected as the optimum. This conclusion was confirmed by the result of the dye removal experiments, conducted by mixing the 0.008g of different synthesized nanofiber to 200mL of BR46 dye solution (30 mg/L) and pH=9 (Table 2). According to the Table 2, increasing the CA content caused to increase the number of Cell NP attached to the surface and resulted to higher adsorption efficiency due to more accessible surface area and functional groups available to the dye on the nanofiber surface. However, the maximum percentage of dye removal decreased when the amount of CA was higher than 0.06g. This can be attributed to a decrease in total adsorbent surface area and an increase in diffusion path length [15].

**Table 2.** The BET surface area value of Cell/Fe<sub>2</sub>O<sub>3</sub> NF synthesized with different amounts of CA

| CA (g)                                | 0.01   | 0.02   | 0.03   | 0.04   | 0.05   | 0.06   | 0.07  | 0.08  |
|---------------------------------------|--------|--------|--------|--------|--------|--------|-------|-------|
| BET surface area (m <sup>2</sup> /g)  | 140.55 | 152.18 | 164.59 | 169.53 | 171.91 | 178.74 | 90.52 | 41.73 |
| Maximum of Dye removal efficiency (%) | 16.16  | 30.14  | 48.87  | 57.54  | 71.27  | 94.55  | 61.28 | 30.36 |

*Effect of operational parameters on dye removal*

*Effect of initial dye concentration.* The effect of initial dye concentration on dye removal was investigated and results are depicted on Fig. 5. It was clear that by raising the initial dye concentration, the dye adsorption efficiency was decreased from 97.22 (20 mg/L) and 94.55% (20 mg/L) to 52.93 (60 mg/L) and 49.93% (60 mg/L) for BR46 and BB41, respectively. However, the adsorption capacity increased from 486.1 (20 mg/L) and 472.75 mg/g (20

mg/L) to 793.95 (60 mg/L) and 748.95 mg/g (60 mg/L) for BR46 and BB41, respectively. It can be concluded that the dye adsorption onto nanofibers increases with an increase in the initial dye concentration. This can be due to the increase in the driving force of the concentration gradient which is stronger at higher amount of initial dye concentration. The optimum initial dye concentration for both BR46 and BB41 were selected as 30 mg/l.

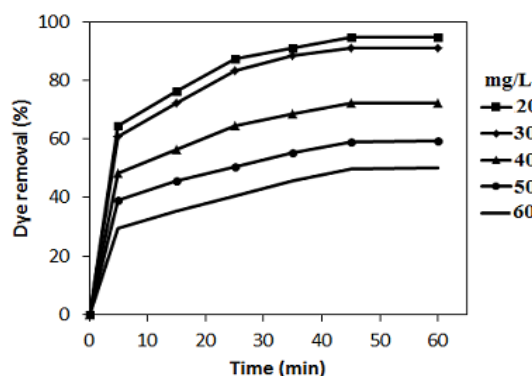
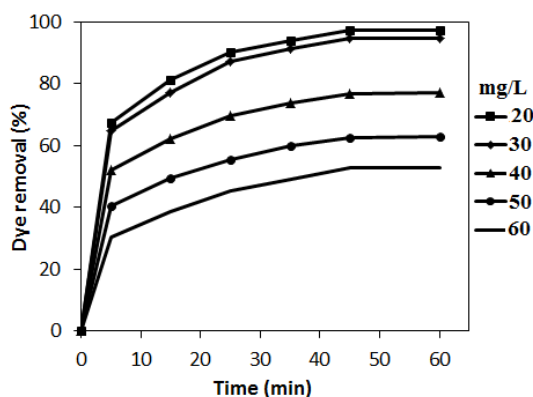


**Fig. 5.** Effect of initial dye concentration on dye removal (A) BR46 (B) BB41

*Effect of adsorbent dosage*

The effect of Cell/Fe<sub>2</sub>O<sub>3</sub> NF dosage on dye removal was investigated and the result is shown in Fig. 6. The dye removal efficiency increased with increasing the nanofiber dosage, which was due to the increase of adsorbent surface area and availability of more adsorption sites against a constant amount of dye molecule. However, increasing in the amount of adsorbent caused to overlapping or aggregation of adsorption sites and

resulted to decrease of the adsorption capacity. The removal efficiencies with the adsorbent dose of 0.008g reached up to 94.55 and 91.1% for BR46 and BB41, respectively. Also, the adsorption efficiencies initially increased and then decreased, which might be due to the large numbers of vacant active sites at the initial stage and then saturated sites hinder the adsorption of remained dye molecules in the solution.

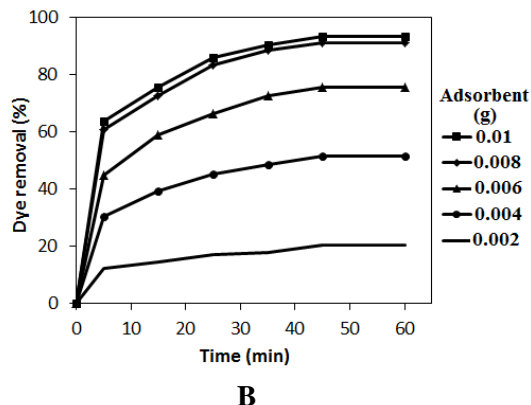
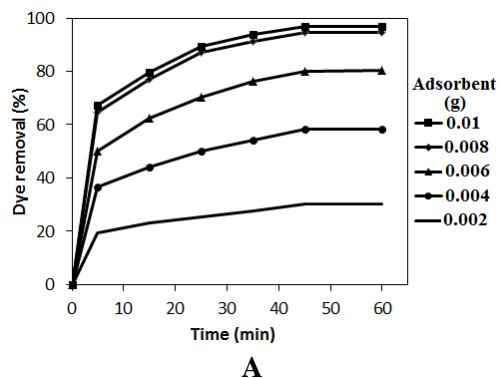


**Fig. 6.** Effect of adsorbents dosage on dye removal (A) BR46 (B) BB41

Effect of pH

The effect of pH on dye removal for different dyes is illustrated in Fig. 7. The maximum adsorption of basic dyes occurred at pH= 9. In the alkaline pH, the nanofiber was deprotonated, and the electrostatic attraction between adsorbent and dye molecules increased resulting in higher dye adsorption. In the acidic pH, the nanofiber was protonated, and the repulsive force between the dye molecules and positively charged nanofiber hinder the adsorption of dye molecule in the solution. Also, the excessive H<sup>+</sup> ions in the solution compete with the dye molecules, resulting in the low dye adsorption. In addition, the effect of pH can be explained by considering the surface charge on nanofiber adsorbent. The point of zero charge (pH<sub>pzc</sub>) of Cell/Fe<sub>2</sub>O<sub>3</sub> NF, determined by the solid addition method was about 5.3 (Fig. 8). When pH <

pH<sub>PZC</sub>, the surface charge is positive, and when pH > pH<sub>PZC</sub>, the surface charge is negative [43]. From the Fig. 8, it was also clear that the solution pH values change during the adsorption process. The final pH (pH<sub>f</sub>) values were higher than the initial pH (pH<sub>0</sub>) values when the pH<sub>0</sub><7.

This is due to an acid neutralization effect and proton adsorption of the surface of nanofiber [44]. The final pH value was in the range of 4.9-5.8 when the initial pH ranges from 3-9. Also, the pH<sub>f</sub> was 7 at the initial pH of 10 .This is an indication of a buffering capacity caused by the adsorbent [45].

In the case of BR46, the removal efficiency was higher than BB41 probably due to the smaller spatial prohibition in the molecular structure and lower molecular weight of BR46 [46] which enable the dye molecule to reach on the surface faster than BB41.

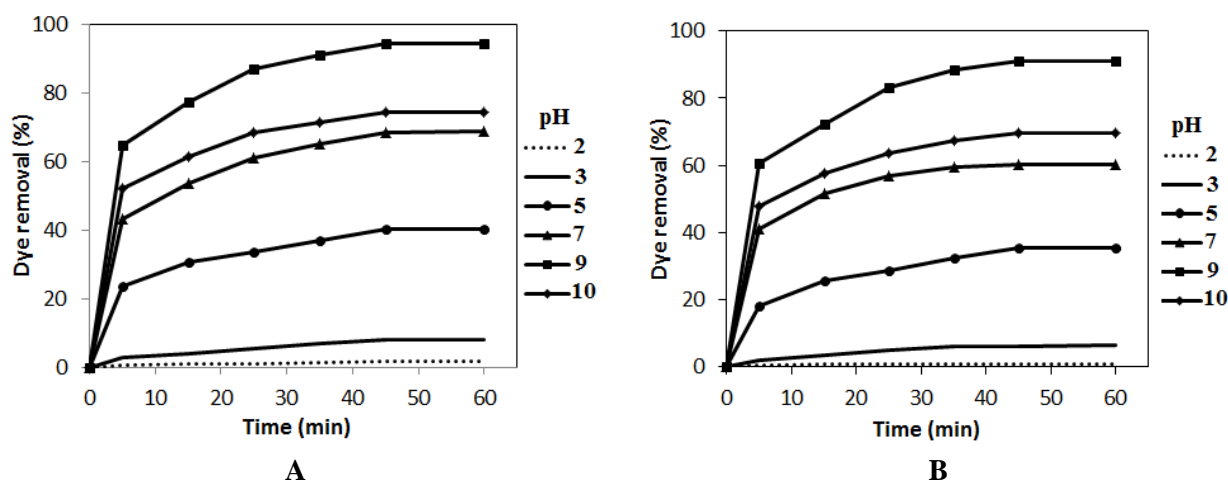


Fig. 7. Effect of pH on dye removal (A) BR46 (B) BB41.

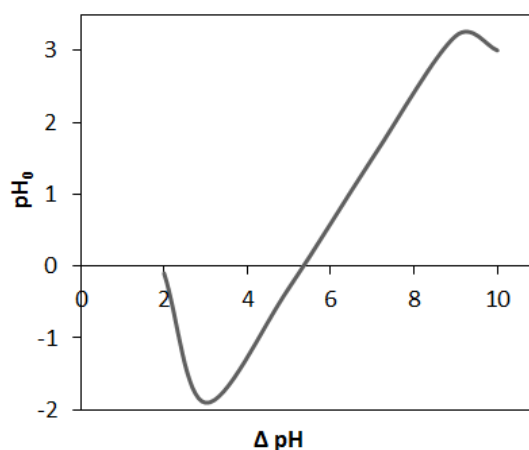


Fig. 8. Δ pH values as a function of initial pH (pH<sub>0</sub>)

The maximum adsorption capacity of α-Fe<sub>2</sub>O<sub>3</sub> nanofiber for BR46 and BB41 in the optimum condition was determined as 39.88 and 38.54 mg/g, respectively. It was clear that incorporation of Cell

NP onto the surface significantly enhance the dye adsorption property of α-Fe<sub>2</sub>O<sub>3</sub> nanofiber.

Adsorption isotherm

Adsorption isotherm is the equilibrium relationship between the concentration of adsorbate

in the liquid phase and the concentration in the adsorbent phase at a given temperature. They indicate on the interaction between adsorbent and adsorbate.

Linear regression is the most common method to determine isotherm parameters. In this method, the best fitted model is typically assessed by the magnitude of the correlation coefficient for the regression. Nevertheless, linearization implicitly alters the error structure and may violate the error variance and normality assumptions of standard least squares. In this study, all the model parameters were evaluated by nonlinear regression.

In order to optimize the procedure an error function need to define to evaluate the fit of the equation to the experimental data. In this study, three different error functions were examined and in each case the isotherm parameters were determined by minimizing the respective error function. The experimental data on the effect of an initial dye concentration on the nanofiber was fitted to the isotherm models using Data fit version 9.0. The error functions were as follow.

1. The chi-squared test ( $\chi^2$ ):

$$\chi^2 = \sum_{i=1}^n \frac{(q_{e,calc} - q_{e,means})^2}{q_{e,means}} \quad (3)$$

2. Average relative error:

$$ARE = \frac{100}{n} \sum_{i=1}^n \left| \frac{q_{e,means} - q_{e,calc}}{q_{e,means}} \right| \quad (4)$$

3. The sum of the squares of the errors (ERRSQ):

$$ERRSQ = \sum_{i=1}^n (q_{e,calc} - q_{e,means})_i^2 \quad (5)$$

where n is the number of observations in the experimental data,  $q_{e,cal}$  is equilibrium capacity obtained by calculation from model (mg/g) and  $q_{e,meas}$  is the equilibrium capacity (mg/g) from the experimental data.

Langmuir, Freundlich and Tempkin isotherms are the most frequently equations used to represent data on adsorption from solution.

The Langmuir isotherm often describes monolayer adsorption with a uniform energy of adsorption on adsorbents. The nonlinear expression

of Langmuir adsorption isotherm can be given as Eq. 6:

$$q_e = \frac{Q_0 K_L C_e}{1 + K_L C_e} \quad (6)$$

where  $q_e$  is the amount of dye adsorbed on the adsorbent at equilibrium (mg/g),  $C_e$  is the equilibrium concentration of dye solution (mg/L),  $K_L$  is the equilibrium constant (L/g), and  $Q_0$  is the maximum adsorption capacity (mg/g).

The Freundlich model imply to multilayer adsorption. This model assumes that there is an exponential variation in site energies of adsorbent. The nonlinear form of Freundlich adsorption isotherm is represented as Eq. 7:

$$q_e = K_F C_e^{\frac{1}{n}} \quad (7)$$

where  $K_F$  is the adsorption capacity at unit concentration and  $\frac{1}{n}$  is the adsorption intensity. The  $\frac{1}{n}$  value ranges between 0 and 1 and it is a measure of surface heterogeneity.

The Temkin isotherm assumes that the heat of adsorption of all the molecules in the layer decreases linearly with coverage due to adsorbent-adsorbate interactions. The Temkin isotherm equation is given as:

$$q_e = \frac{RT}{b \ln(K_T C_e)} \quad (8)$$

$K_T$  is the equilibrium binding constant (L/mol) corresponding to the maximum binding energy and constant  $B_1$  is related to the heat of adsorption. Also, T is the absolute temperature (K), and R is the universal gas constant (8.314 J · mol<sup>-1</sup> K<sup>-1</sup>). The coefficient values for various isotherms and values of different errors from nonlinear method are listed in Tables 3 and 4.

From the Table 3, it was concluded that the Langmuir model has a better fit to experimental data. The high values of R<sup>2</sup> (>0.99) suggest the applicability of Langmuir model to the adsorption process. Also, the error values of three different error functions imply on a better fit of Langmuir model to the experimental data. It was concluded that the adsorbent surface is homogeneous in character and formation of monolayer takes place on the surface of the adsorbent.

**Table 3.** The coefficient values for various isotherms

| Dye         | Langmuir       |                |                | R <sup>2</sup> | Freundlich |                | Tempkin        |                |                |
|-------------|----------------|----------------|----------------|----------------|------------|----------------|----------------|----------------|----------------|
|             | R <sup>2</sup> | Q <sub>0</sub> | K <sub>L</sub> |                | 1/n        | K <sub>F</sub> | R <sup>2</sup> | B <sub>1</sub> | K <sub>T</sub> |
| <b>BB41</b> | 0.999          | 757.57         | 1.975          | 0.735          | 0.119      | 528.91         | 0.815          | 59.57          | 6825.63        |
| <b>BR46</b> | 0.999          | 800            | 3.778          | 0.798          | 0.108      | 592.82         | 0.832          | 69.58          | 7258.64        |



## Adsorption kinetic

To design an effective adsorption system, investigations on adsorption rate are essential. The kinetic studies are helpful for the prediction of the adsorption rate and they give important information about the mechanism of solute sorption onto a sorbent. In order to determine the kinetics

parameters, nonlinear regression was used due to prevent from inherent bias resulting from the linearization. In this study, the pseudo-first-order, pseudo-second-order and intra-particle diffusion kinetic models were tested to interpret the experimental kinetic data.

**Table 4.** Values of different errors from nonlinear method

| Dye  | Isotherm models | Chi-square ( $\chi^2$ ) | Average relative error (ARE) | The sum of the squares of the errors (ERRSQ) |
|------|-----------------|-------------------------|------------------------------|--|
| BR46 | Langmuir        | 0.678                   | 2.587                        | 8.257  |
|      | Freundlich      | 1.925                   | 29.774                       | 202.174                                      |
|      | Tempkin         | 2.886                   | 35.472                       | 241.853                                      |
| BB41 | Langmuir        | 0.882                   | 2.104                        | 10.258                                       |
|      | Freundlich      | 2.587                   | 28.218                       | 198.668                                      |
|      | Tempkin         | 4.185                   | 30.532                       | 274.628                                      |

The non-linearized form of pseudo-first order equation is expressed as:

$$q_t = q_e [1 - \exp(-k_1 \times t)] \quad (9)$$

where  $q_e$  is the amount of dye adsorbed at equilibrium ( $mg / g$ ),  $q_t$  is the amount of dye adsorbed at  $t$  time ( $mg / g$ ) and  $K_1$  is the equilibrium rate constant of pseudo-first-order adsorption ( $min^{-1}$ ).

The non-linear form of pseudo-second order kinetic model is as follows:

$$q_t = \frac{k_2 \times t \times q_e^2}{(1 + k_2 \times t \times q_e)} \quad (10)$$

$K_2$  is the pseudo-second order equilibrium rate constant ( $g / mg \text{ min}$ ).

The intra-particle diffusion model can be represented as:

$$q_t = k_p t^{\frac{1}{2}} + I \quad (11)$$

where  $k_p$  and  $I$  are the intra-particle diffusion rate constant and intercept, respectively.

In order to find out the most suitable kinetic models for representing the experimental data, non-linear regression along with 3 error functions (chi-squared test, Average relative error and the sum of the squares of the errors) were used. The parameters of different kinetic models and different errors values were calculated by Data fit version 9.0 and the results are shown in Table 5.

Table 5 illustrated that the correlation coefficient ( $R^2$ ) of the pseudo-second-order kinetic model was very close to 1 and its error function values was lower than pseudo-first-order kinetic and intra particle models.

It can be concluded that the rate of adsorption follows pseudo-second order rate equation.

**Table 5.** The parameters of different kinetic models and different errors from nonlinear model

| Dye                       | BR46    | BB41    |
|---------------------------|---------|---------|
| Pseudo-first-order model  |         |         |
| $R^2$                     | 0.813   | 0.804   |
| $(q_e)_{Cal}$             | 882.36  | 835.91  |
| $K_1$                     | 0.142   | 0.139   |
| $\chi^2$                  | 8.204   | 8.628   |
| ARE                       | 20.146  | 18.986  |
| ERRSQ                     | 244.262 | 302.587 |
| Pseudo-second-order model |         |         |
| $R^2$                     | 0.997   | 0.998   |
| $(q_e)_{Cal}$             | 792.25  | 730.78  |
| $K_2 \times 10^{-2}$      | 3.288   | 2.426   |
| $\chi^2$                  | 0.468   | 0.604   |
| ARE                       | 5.852   | 6.366   |
| ERRSQ                     | 10.114  | 10.087  |
| Intraparticle diffusion   |         |         |
| $R^2$                     | 0.840   | 0.825   |
| $k_p$                     | 85.97   | 79.58   |
| $I$                       | 165.82  | 158.77  |
| $\chi^2$                  | 8.485   | 8.779   |
| ARE                       | 19.222  | 20.478  |
| ERRSQ                     | 298.108 | 303.811 |

## Comparison with other adsorbents

The maximum adsorption capacity of Cell/Fe<sub>2</sub>O<sub>3</sub> NF for BR46 and BB41 with other previously prepared adsorbents is presented in Table 6. It was

obvious that Cell/Fe<sub>2</sub>O<sub>3</sub> NF has higher adsorption capacity in comparison to the previous adsorbent [47- 52].

**Table 6.** The maximum adsorption capacity of cell-g-Fe<sub>2</sub>O<sub>3</sub> nanofiber for BR46 and BB41 with other previously prepared adsorbents

| Adsorbent  | Adsorption capacity(mg/g) | Dye                    | Ref           |
|--|---------------------------|------------------------|---------------|
| polyaniline/zirconium oxide<br>carboxylate group | 77.51                     | BR46                   | 47            |
| functionalized single-walled<br>carbon nanotube  | 140                       | BR46                   | 48            |
| Silica nanoparticle                              | 88                        | BR46                   | 49            |
| cellulose-based adsorbent                        | 175.43                    | Crystal violet         | 50            |
| Modified mesoporous clay                         | 62.5                      | Methylene blue<br>(MB) | 51            |
| Chitosan–clay composite                          | 259.81                    | Methylene blue<br>(MB) | 52            |
| Cell/Fe <sub>2</sub> O <sub>3</sub> NF           | 800<br>757.57             | BR46<br>BB41           | Current study |

## CONCLUSION

In this paper, Cell/Fe<sub>2</sub>O<sub>3</sub> nanofiber was synthesized and its dye removal ability was investigated. The optimum amount of citric acid, used as crosslinking agent was 0.06g in the incorporation of Cell NP process. The FTIR result illustrated that Cell NP was crosslinked together through an esterification process. Then, they were incorporated onto the nanofiber surface because of the interactions among functional groups of cellulose and inorganic coated nanofibers. SEM images confirmed the incorporation of cell NP with the average diameter of 35.2nm on the surface of nanofibers. Also, BET surface area increased after the incorporation of Cell NPs on the surface due to high BET surface area value of Cell NPs.

The adsorption experiments indicated that the incorporation of Cell NP onto the surface of inorganic nanofiber drastically increased the dye adsorption property. Also, the result showed that the maximum of dye removal occurred at alkaline pHs due to presence of high amounts of hydroxyl group on the nanofiber surface. The investigation on adsorption isotherm and kinetic models were performed by non-linear regression and 3 error functions. The results revealed that adsorption follows the Langmuir isotherm, indicated on the formation of monolayer on the surface of the nanofiber. Also, the adsorption kinetic of dyes conforms to pseudo-second-order model.

## REFERENCES

1. F. Liu, B. Ma, D. Zhou, L. J. Zhu, Y. Y. Fu, L. X. Xue, *React. Funct. Polym.*, **86**, 191 (2015).
2. J. Wu, L. Ma, Y. Chen, Y. Cheng, Y. Liu, X. Zha, *Water. Res.*, **92**, 140 (2016).
3. A. Kumar Verma, R. Roshan Dash, P. Bhunia, *J. Environ. Manag.*, **93**, 154 (2012).
4. A. Maljaei, M. Arami, N. M. Mahmoodi, *Desalin.* **249**, 1074 (2009).
5. K. Natarajan, H. C. Bajaj, R. J. Tayade, *J. Ind. Eng. Chem.*, **34**, 146 (2016).
6. A. Almasiana, M. Parvinzadeh Gashtib, M. E. Olya, G. Chizarifard, *Desalin. Water Treat.*, **55**, 1 (2016).
7. V. S. Mane, P. V. Vijay Babu, *Desalin.* **273**, 321 (2011).
8. X. L. Zhao, J. M. Wang, F. C. Wu, T. Wang, Y. Q. Cai, Y. L. Shi, G. B. Jiang, *J. Hazard. Mater.* **173**, 102 (2010).
9. J. M. Gómez, J. Galán, A. Rodríguez, G. M. Walker, *J. Environ. Manag.*, **146**, 355 (2014).
10. P. Pengthamkeerati, T. Satapanajaru, *Desalin. Water Treat.*, **54**, 227 (2015).
11. T. Zehra, N. Priyantha, L. B. Lim, E. Iqbal, *Desalin. Water Treat.*, **54**, 2592 (2015).
12. W. Tze Mook, M. Kheireddine, M. Szlachta, *Bioresour.*, **11**, 1432 (2016).
13. P. Sharma, D. J. Borah, P. Das, M. R. Das, *Desalin. Water Treat.*, **57**, 8372 (2016).
14. N. M. Mahmoodi, R. Salehi, M. Arami, H. Bahrami, *Desalin.*, **267**, 64 (2011).
15. N. M. Mahmoodi, *J. Chem. Eng. Data.*, **56**, 2802 (2011).
16. W. Wu, Q. He, C. Jiang, *Nanoscale. Res. Lett.*, **3**, 397 (2008)
17. E. Kumar, A. Bhatnagar, W. Hogland, M. Marques, *Adv. Colloid. Interf.*, **203**, 11 (2014).
18. N. M. Mahmoodi, *J. Environ. Eng.* **139**, 1382 (2013).
19. S. Kango, S. Kalia, A. Celli, J. Njuguna, Y. Habibi, R. Kumar, *Progr. Polym. Sci.*, **38**, 1232 (2013).
20. A. M. Donia, A. A. Atia, W. A. Alamrani, A. M. El-Nahas, *J. Hazard. Mater.* **161**, 1544 (2009).

21. N. M. Mahmoodi, S. Khorramfar, F. Najafi, *Desalin.*, **279**, 61 (2011).
22. A. Yousefzadi Nobakht, and S. Shin, *J. Appl. Phys.* **120**, 225111 (2016).
23. T. J. Daou, J. M. Grenèche, G. Pourroy, S. Buathong, A. Derory, C. Ulhaq-Bouillet, B. Donnio, D. Guillon and S. B. Colin, *Chem. Mater.*, **20**, 5869 (2008).
24. A. Gupta, V. Singh Chauhan, N. Sankararamkrishnan, *Water. Res.* **43**, 3862 (2009).
25. X. Liu, Q. Hu, Z. Fang, X. Zhang and B. Zhang, *Langmuir.*, **25**, 3 (2009).
26. T. S. Anirudhan M. Ramachandran, *Appl. Clay. Sci.*, **35**, 276 (2007).
27. G. Zeng, Y. Liu, L. Tang, G. Yang, Y. Pang, Y. Zhang, Y. Zhou, Z. Li, M. Li, M. Lai, X. He, Y. He, *Chem. Eng. J.*, **259**, 153 (2015).
28. S. Hokkanen, E. Repo, S. Lou, M. Sillanpää, *Chem. Eng. J.*, **260**, 886 (2015).
29. S. Hosseini, A. Shamekhi, and A. Yazdani, *J. Renew. Sust. Ener.* **4**, 043107 (2012).
30. S. P. Akhlaghi, M. Zaman, N. Mohammed, C. Brinatti, R. Batmaz, R. Berry, W. Loh, K. Chiu Tam, *Carbohydr. Res.*, **409**, 48 (2015).
31. T. S. Anirudhan, Tharun A. Rauf, *J. Ind. Eng. Chem.*, **19**, 1659 (2013).
32. T. Ren, P. He, W. Niu, Y. Wu, L. Ai, X. Gou, *Environ. Sci. Pollut. Res.*, **20**, 155 (2013).
33. A. Hamidi, and S. Jedari, *Sharif. Civ. Eng. J.* **29**, 29-35 (2011).
34. A. Ghaee, M. Shariaty-Niassar, J. Barzin, A. Zarghan, *Appl. Surf. Sci.*, **258**, 7732 (2012).
35. N. Wang, E. Ding, R. Cheng, *Langmuir.*, **24**, 5 (2008).
36. L. Ai, C. Zhang, F. Liao, Y. Wang, M. Li, L. Meng, J. Jiang, *J. Hazard. Mater.*, **198**, 282 (2011).
37. X. Jun, S. Xiang-Qian, S. Fu-Zhan, L. Ming-Quan, *Chin. Phys. B*, **18**, 181 (2009).
38. P. Satyamurthy, P. Jain, R.H. Balasubramanya, N. Vigneshwaran, *Carbohydr. Polym.*, **83**, 122 (2011).
39. S. Y. Oh, D. I. Yoo, Y. Shin, G. Seo, *Carbohydr. Res.*, **340**, 417 (2005).
40. M. Parvinzadeh Gashti, A. Almasian, *Compos. Part B Eng.*, **43**, 3374 (2012).
41. C. Yang, B. K. Andrews, *J. Appl. Polym. Sci.*, **43**, 1609 (1991).
42. V. Ameri Dehabadi, H. J. Buschmann, J. Stefan Gutmann, *Textile. Res. J.*, **83**, 1974 (2013).
43. S. Yari, S. Abbaszadeh, S. E. Mousavi, M. Saei Moghaddam, A. Zarringhalam Moghaddam, *Proc. Safet. Environ. Protect.*, **94**, 159 (2015).
44. V. S. Mane, P. V. V. Babu, *Desalin.*, **273**, 321 (2011).
45. V. C. Srivastava, M. M. Swamy, I. D. Mall, B. Prasad, I. M. Mishra, *Physicochem. Eng. Aspec.* **272**, 89 (2006).
46. L. Eskandarian, M. Arami, E. Pajootan, *J. Chem. Eng. Data.*, **59**, 444 (2014).
47. S. Agarwal, I. Tyagi, V. Kumar Gupta, F. Golbaz, A. Nozad Golikand, O. Moradi, *J. Mol. Liquids*, **218**, 494 (2016).
48. A. Yousefzadi Nobakht, and S. Shin, *J. Appl. Phys.* **120**, 225111 (2016).
49. N. M. Mahmoodi, A. Maghsoodi, *Desalin. Water. Treat.*, **54**, 562 (2015).
50. Y. Zhou, M. Zhang, X. Wang, Q. Huang, Y. Min, T. Ma, J. Niu, *Ind. Eng. Chem. Res.* **53**, 5498 (2014).
51. M. Auta, B. H. Hameed, *Chem. Eng. J.*, **219**, 198, (2012).
52. M. Auta, B.H. Hameed, *Chem. Eng. J.*, **237**, 352 (2014).